

Hinode EUV Study of Jets in the Sun's South Polar Corona

Len CULHANE, Louise K. HARRA, Deborah BAKER, Lidia VAN DRIEL-GESZTELYI, and Jian SUN
Mullard Space Science Laboratory, University College London, Holmbury St. Mary, Dorking, Surrey RH5 6NT, UK
jlc@mssl.ucl.ac.uk

George A. DOSCHEK and David H. BROOKS
Space Science Division, Naval Research Laboratory, 4555 Overlook Avenue, SW, Washington, DC, 20375, USA

Loraine L. LUNDQUIST
Smithsonian Astrophysical Observatory, 60 Garden Street, Cambridge, MA 02138, USA

Suguru KAMIO
National Astronomical Observatory of Japan, 2-21-1 Osawa, Mitaka, Tokyo 181-8588

Peter R. YOUNG
STFC, Rutherford Appleton Laboratory, Harwell Science and Innovation Campus, Didcot, OX11 0QX, UK
and

Viggo H. HANSTEEN
Institute of Theoretical Astrophysics, University of Oslo, P.O.Box 1029 Blindern, N-0315 Oslo, Norway

(Received 2007 June 4; accepted 2007 September 6)

Abstract

A number of coronal bright points and associated plasma jet features were seen in an observation of the South polar coronal hole during 2007 January. The 40'' wide slot was used at the focus of the Hinode EUV Imaging Spectrometer to provide spectral images for two of these events. Light curves are plotted for a number of emission lines that include He II 256 Å (0.079 MK) and cover the temperature interval from 0.4 MK to 5.0 MK. Jet speed measurements indicate values less than the escape velocity. The light curves show a post-jet enhancement in a number of the cooler coronal lines indicating that after a few minutes cooling, the plasma fell back to its original acceleration site. This behavior has not been previously observed by e.g., the Yohkoh Soft X-ray Telescope due to the comparatively high temperature cut-off in its response. The observations are consistent with the existing models that involve magnetic reconnection between emerging flux and the ambient open field lines in the polar coronal hole. However we do not have sufficient coverage of lines from lower temperature ion species to register the H α -emitting surge material that is associated with some of these models.

Key words: Sun: atmospheric motions — Sun: corona — Sun: UV radiation

1. Introduction

Soft X-ray jets, roughly collimated flows of high temperature plasma, were discovered in Yohkoh/SXT data (Shibata et al. 1992; Strong et al. 1992). Supported by MHD simulations (Yokoyama & Shibata 1995, 1996) it is generally accepted that the jets are caused by magnetic reconnection between emerging flux and ambient open or far-reaching magnetic field lines. The detailed topology depends on whether the ambient flux is near-vertically directed or close to horizontal. Building on earlier suggestions by Sterling et al. (1991), Sterling, Shibata, and Mariska (1993, 1994), Shimojo and Shibata (2000) provided evidence for the jets being consistent with evaporation flows produced by the reconnection heating. Magnetic reconnection between closed (emerging) and open field lines, besides the jet, is expected to create a new closed loop, which can be observed as a (flaring) bright point in the vicinity of the jet. Such flaring bright points have indeed been found in association with the majority of X-ray jets (Shimojo et al. 1996). Flaring from the closed loop bright points has also been observed in EUV filter observations (e.g., Brooks et al. 2007).

Yokoyama and Shibata (1995) showed two possible schemes

for the interaction of emerging magnetic flux depending upon whether the ambient field is near vertical or horizontal (see their figures 3c and 3d). Since the work reported here describes jets that appear in a coronal hole near the limb and in the Sun's South polar region, we would anticipate that the emerging flux interaction is likely to involve reconnection with near-vertical open field lines in the coronal hole. Thus the resulting jet will be directed outwards from the Sun in a near-vertical direction and the topology will be closer to that shown schematically in figure 3c of Yokoyama and Shibata. In a companion paper in the present issue, Kamio et al. (2007) report observations of bright points and jets in the North polar region on 2007 January 9. Their data were acquired also using the EUV Imaging Spectrometer (EIS) instrument (Culhane et al. 2007) onboard Hinode (Kosugi et al. 2007) with its one arc sec slit selected to obtain rastered images in nine different spectrum lines. Their paper describes the resulting velocity measurements at the base of a jet and in the neighborhood of its associated bright point.

In the present work we have used the EIS 40'' slots at the instrument focus. While the extension of 40'' in the dispersion direction inevitably leads to spectral/spatial convolution, the resulting images are obtained in a time-coherent manner and can track solar features and events with a time cadence set

in the instrument. In some cases it is possible to select spectral ranges that are largely free of emission lines other than the one selected for observation. In other cases where the additional lines are weak at the plasma temperatures involved, their contribution may be ignored.

This paper describes spectral images that were obtained for two jets. One of our longer term goals is to identify the source and ultimate fate of the plasma involved in these events and we will report some progress in this area. After a discussion of the data analysis methods, we describe a study of fourteen different emission line images and a representative image (Fe XV) is presented. The results are compared with images obtained using the Hinode X-ray Telescope (XRT; Golub et al. 2007). The EIS observations together with an estimate of jet volume allow rough estimates of jet temperature and electron density to be obtained. Light curves are plotted against time for each line emitted by the jets and associated bright point plasma. So far as we are aware, this is the first occasion on which coronal X-ray jet plasma has been studied over such a wide range of ion species and temperatures.

2. Data and Analysis

The observational study used employed the EIS $40'' \times 512''$ slot. The image pixels are of $1''$ size thus slightly undersampling the $2''$ instrument resolution. In order to enhance the spatial coverage, a three position raster was used to cover a total area of $120'' \times 512''$ at a three minute time cadence. The exposure time for each slot image was one minute. Each EIS FITS file, containing data for all 14 emission lines, was prepared using the SolarSoft (SSW) XFILES tool and the `eis_prep` routine within IDL. The FITS files were calibrated by selecting default dark current (DC), cosmic ray (CR), and absolute calibration (abs) options within the EIS calibration control window. The selected EIS raster step size was $38''$ and hence two of the three $40''$ slot images were cropped before being rotated and combined to construct a final EIS image for each line. In addition to the EIS slot images, $1024'' \times 512''$ XRT images of $1''$ pixels and ≈ 30 s time cadence were used. XRT FITS files were prepared and calibrated using the SSW `xrt_prep` routine. A map structure was created from each EIS and XRT image using standard SSW routines. EIS and XRT maps were derotated to 2007 January 20, 15:02 UT for Jet 1 (see figure 1) and 16:02 UT for Jet 2 (see figure 2).

Jet intensities were obtained using the SSW `defroi` routine to fit a contour defined by eye around each jet or bright point in an image at the time when the particular feature was at its largest extent. Intensity was summed within the contour region for each EIS line image and XRT image. In the case of EIS, contours for line images for the $170 \text{ \AA} - 210 \text{ \AA}$ (CCD B) were shifted 18 pixels in the negative Y -direction to correct a detector misalignment. The amount of this shift was determined by aligning well-defined solar features and the southern solar limb in line images from both detectors.

Light curves for the two jets and associated bright points were constructed by subtracting pre-event averaged background within the contour region for each EIS line image and XRT image. The averaged background values were

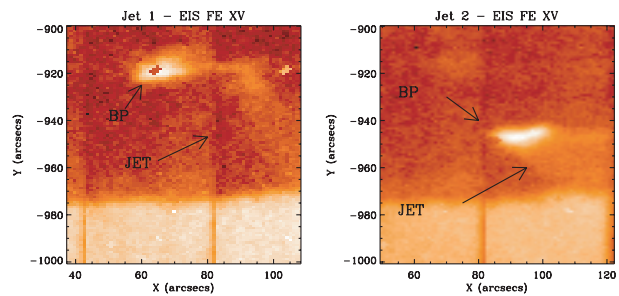


Fig. 1. EIS Fe vx slot observations of the two jets. Jet 1 was observed between 15:00 UT and 16:00 UT on 2007 January 20. Jet 2 was observed between 16:30 UT and 17:20 UT on the same date. Arrows indicate the jet and its associated bright point (BP).

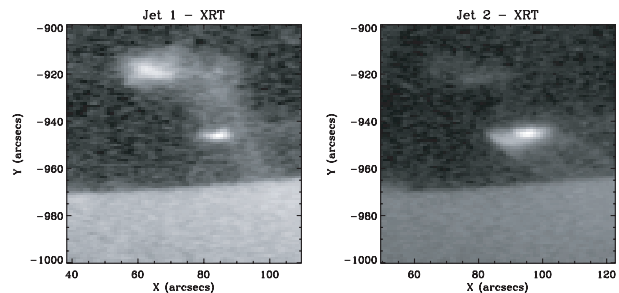


Fig. 2. Hinode/XRT observations of the two jets using the Al Poly filter.

calculated for the same pre-event time period for both EIS and XRT fluxes. Averaged background for Jet 1 was calculated for the interval 14:50 UT to 14:59 UT while for Jet 2, the relevant time interval was 16:21 UT to 16:27 UT. The complete data series for this study runs from 14:50 UT to 17:24 UT on 2007 January 20.

3. Observations

The 14 lines used to obtain the slot images that are discussed in the paper are listed in table 1. Ion species, line wavelength, and the temperature corresponding to the peak of the $G(T_e)$ curve (includes the T_e -dependent parts) for transition excitation are given in the first three columns. Details of the transitions are given in e.g., Dere et al. (1997).

With a dispersion of about 0.023 \AA per arc sec pixel, the $40''$ wide slot images correspond to a total wavelength range of 0.92 \AA or $\pm 0.46 \text{ \AA}$ on each side of the prime slot lines. The ions with transitions in these ranges are shown for each of the prime lines in the fourth column. The final column of the table indicates the colour coding of the light curves used in later figures to represent the jet fluxes. Lines observed by EIS in typical Quiet Sun and Active Region spectra are included in the table. Although the He II line at 256.32 \AA is strong in the transition region, its excitation mechanism is not well understood and in any case it is associated with ions from a wide range of coronal temperatures in a slot image. For the Fe XV transition at 284.16 \AA , the only other transition is from Al IX — an ion present at 1 MK. Thus if the Fe X line at 184.54 \AA (also formed at 1 MK) is absent, we can be confident

Table 1. Emission lines used in EIS jet study.

Ion species	λ (Å)	T_e (MK)	Other ions with transitions in the 40'' slot range (AR, QS)	Light curve – colour code
He II	256.32	0.079	Si X, Fe XII, Fe XIII, Ni XVI, S XIII	Black – solid
Si VII	275.35	0.63	Si VII lines	Purple – solid
Si X	261.04	1.26	No other lines	Yellow – solid
Fe XII	195.12	1.26	Fe VIII, Ni XVI, Ni XV	Red – solid
Fe XIII	202.04	1.58	Ar XIII	Green – solid
Fe XIV	274.20	2.00	Si VII	Royal Blue – solid
Fe XV	284.16	2.00	Al IX	Light Blue – solid
Fe XI	188.23	1.26	Fe XI, Fe XII	Black – dotted
Ca XVII	192.82	5.01	Fe XI, O V	Black – dashed
Fe XVI	262.98	2.51	No other lines	Black dash/dot
Fe X	184.54	1.00	Ar XI, Fe XI	Red – dashed
Fe VIII	185.21	0.40	Ni XVI	Green – dashed
Si X	258.37	1.26	Si IX	Royal Blue – dashed
Fe XIV	264.79	2.00	Fe XVI	Light Blue – dashed

that the photons registered from a jet are due to the Fe XV transition.

EIS and XRT images of the two jets considered are given in figures 1 and 2. For the EIS images, the three 40'' slot images that have been joined to form the overall image are clearly visible. The jets are at their maximum extent in these images. In all four panels of figures 1 and 2, we can see the classic structure of the jet and its associated bright point.

Using the signal within the selected contours we have plotted intensity against time or light curves for the Jet 1 bright point and for the jet itself (figures 3 and 4) while similar data for Jet 2 are given in figures 5 and 6. The EIS light curves are shown in the left panels while the XRT light curves are in the right panels. The plots are colour coded as specified in table 1 and the significant ions are explicitly labelled.

As remarked above, He II (256 Å) is a complex line given its poorly understood excitation mechanism and its blending with several other lines in the EIS slot. However for both jets, it shows clear impulsive behaviour in the main phase of the signal while becoming weaker and more erratic later. The early impulse in this line may indicate a transition region response to the jet energy release while its low temperature of 0.079 MK for peak ion abundance suggests that it will not be emitted in coronal plasma at temperatures of around 1 MK.

EIS Jet 1 shows early impulsive behaviour in the hotter lines e.g., Fe XIV, Fe XV which then decay. In contrast, in the time interval following the main jet and after an interval of around three to five minutes, the cooler lines e.g., Fe VIII, Fe X, and Fe XII, show gradual increases before they too decay at around 15:58 UT. The XRT light curve (figure 4, right panel) shows clear impulsive jet behaviour. However close inspection reveals a slight gradual rise in the post-jet time interval.

Light curves for the EIS bright point (BP 1) associated with Jet 1 are shown in the left panel of figure 3. These show impulsive behaviour in He II, the hotter lines (Fe XIV, Fe XV) and the cooler lines (Si X) and thus have the appearance associated with a small flare. It is noteworthy that both Jets 1 and 2 show the same start and peak times as their associated bright points, a feature that would be expected from

the reconnection hypothesis. This lends further support to the findings of Shibata et al. (1992) who predicted this close connection.

For Jet 2, the impulsive features are similar to those seen in Jet 1 namely He II and the hotter lines (Fe XIV, Fe XV) rise sharply. However the post jet increase in the cooler lines (Fe XI, Fe XII, Fe XIII) is significantly more pronounced while the latter two lines begin to rise somewhat before the main jet impulse. In this case also there is a small but noticeable post jet response in the XRT signal. Such a signature has to our knowledge never been observed in Yohkoh SXT X-ray jet observations.

Light curves for the associated EIS and XRT BP 2 are shown in figure 5. Similar impulsive behaviour in a range of hotter and cooler lines is observed in this case also. In addition there is a post main phase increase in the cooler lines e.g., Fe VIII, Fe X, similar to that seen following the jet.

Based on simple approximations, it is possible to make a rough estimate of the electron density value for the jet plasma. We assume that all of the detected photons in the 284 Å window come from the Fe XV line at 284.16 Å and are emitted at the peak temperature of the $G(T_e)$ curve for this ion species, namely 2.0 MK. We have taken the photospheric iron abundance value of 3.16×10^{-5} and a filling factor of unity for the jet material. The measured jet volume is $3.2 \times 10^{27} \text{ cm}^3$. The atomic parameters and ion species concentration for the assumed temperature are from the CHIANTI data base (Version 4: Dere et al. 1997; Young et al. 2003). The resulting jet plasma density estimate of $4 \times 10^9 \text{ cm}^{-3}$ is consistent with the range of values determined by Shimojo and Shibata (2000) in their study of 16 X-ray jets observed with Yohkoh SXT. The presence of Fe XIV and Fe XV emission from the jet plasma suggests a temperature of around two to three MK which is again consistent with the average values presented by Shimojo and Shibata.

4. Discussion and Conclusions

Both jets discussed show post-jet increases in their light-curves, which, from the temperature of the lines in which

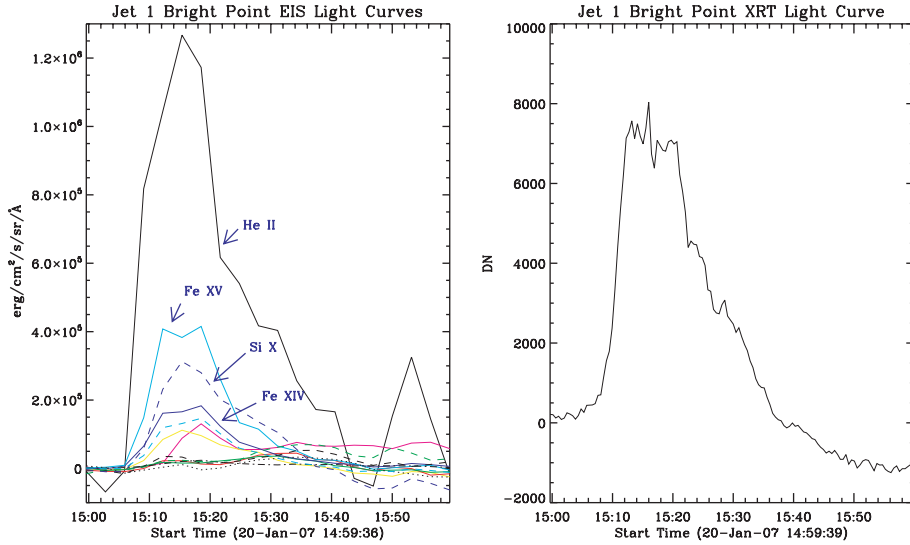


Fig. 3. Light-curves of the bright point (BP) associated with Jet 1; EIS multi-line plot (left) and XRT soft X-ray plot (right). For details of the spectral lines used in the EIS plot see table 1.

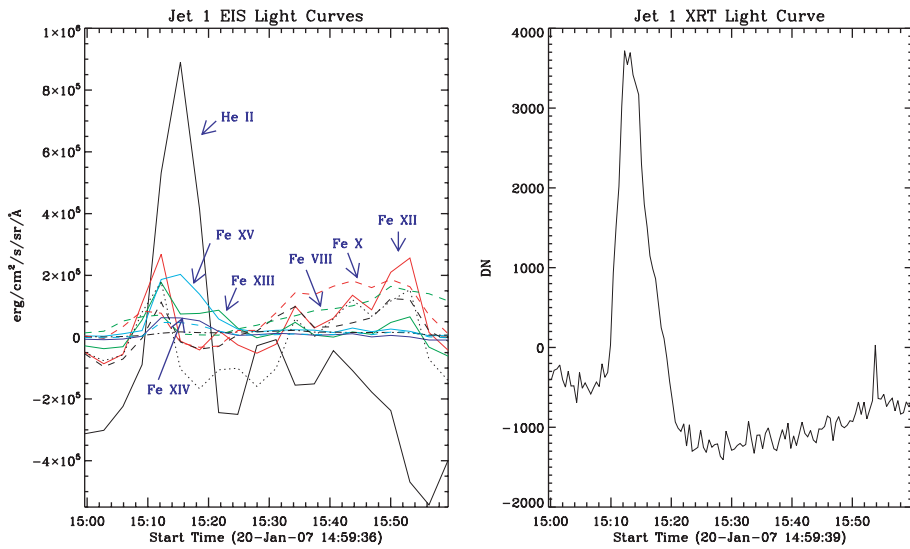


Fig. 4. Light-curves of Jet 1, EIS multi-line plot (left) and XRT soft X-ray plot (right). For details of the spectral lines used in the EIS plot see table 1. Note the post-jet intensity rise in the EIS light-curves.

they appear, look systematically cooler than the jets they follow. Although there is also some evidence for this behavior in the present XRT light curves, it has not been seen in Yohkoh SXT jet observations. A possible explanation for these features may be because the hot plasma, which was propelled upward in the jet, has velocity significantly below what is required to escape from the Sun. Initially the accelerated jet plasma leaves the contour over which we integrated the jet light-curves. Having failed to reach escape speed from the Sun, the material falls back some minutes later in a cooler state and re-enters the contour leading to a secondary increase of intensity in the light-curves that is seen in lines from lower temperature ions.

In order to establish whether the fall-back of jet plasma is possible, we measured the jets' extension speed in the EIS Fe XV images. We measured the extending X-ray jet in EIS

images assuming that the apparent velocity of the extension represents the bulk velocity of the ejected plasma. We found 360 km s^{-1} for Jet 1 and 150 km s^{-1} for Jet 2, all well below the escape velocity of 618 km s^{-1} . The above velocity values agree well with the speeds found by Shimojo et al. (1996) which were in the $10\text{--}1000 \text{ km s}^{-1}$ range with an average of 200 km s^{-1} . For a plasma at $T_e \approx 2 \text{ MK}$, the figure for Jet 2 is less than the local sound speed whereas that for Jet 1 is significantly greater. It is noteworthy that in their sample of 100 jets only five had velocities close to or above the escape velocity from the Sun. Hence it seems to be likely that most of the hot material seen in X-ray jets never escapes from the Sun and so it is surprising that similar post-jet enhancements in the light-curves have not previously been reported.

Ko et al. (2005) have analysed a prominent jet on the solar

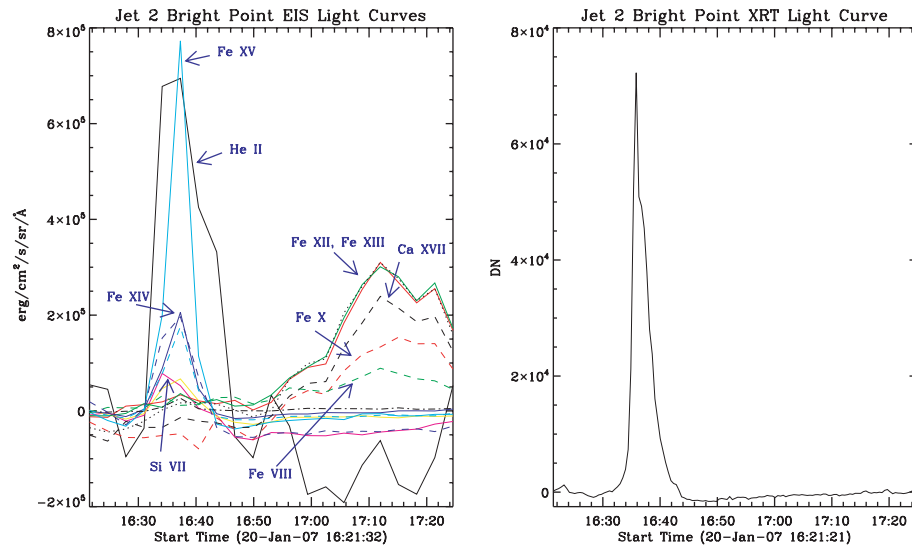


Fig. 5. Light-curves of the bright point (BP) associated with Jet 2; EIS multi-line plot (left) and XRT soft X-ray plot (right). Note the post-jet intensity rise in the EIS light-curves. For details of the spectral lines used in the EIS plot see table 1. In particular, the Ca XVII line is blended with a Fe XI line. The post-jet intensity increase in this blended line is dominated by Fe XI.

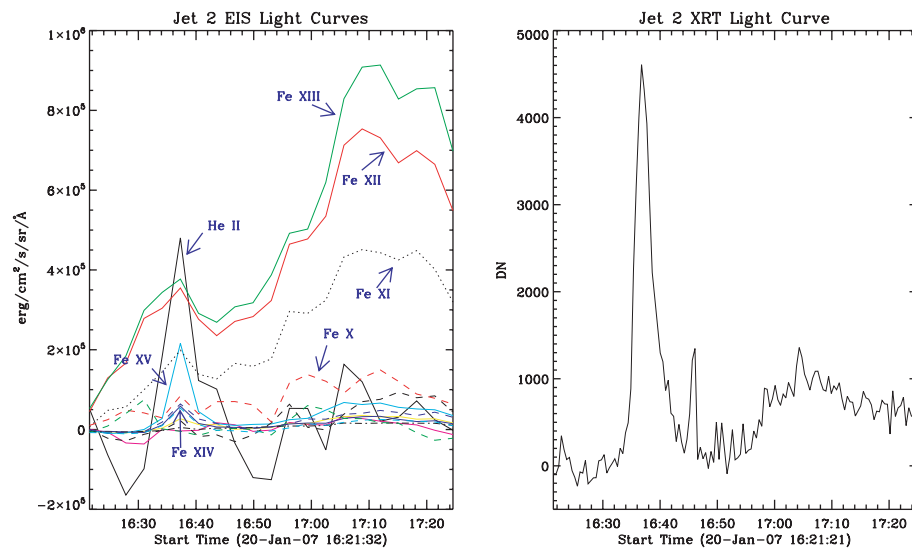


Fig. 6. Light-curves of Jet 2; EIS multi-line plot (left) and XRT soft X-ray plot (right). For details of the spectral lines used in the EIS plot see table 1. Note the post-jet intensity rise in the EIS and XRT light-curves.

limb using SOHO/CDS, EIT and UVCS as well as TRACE, Mauna Loa CHIP and PICS data. They found cool and hot components in the jet. The cool component was maintained for about an hour, while the hot one ceased after about 20 minutes. They also found a reversal in the line-of-sight Doppler signal during the evolution of the jet. The jet velocity in the plane of the sky was found to be below escape speed and the jet was not seen at or above $2.3 R_{\odot}$. Ko et al. (2005) concluded that a falling-back scenario was consistent with their observations, which supports our finding.

To our knowledge this kind of gradual enhancement in cooler coronal lines has not been observed following normal flare events. Short term transient enhancements in lines of He I, O V, and Mg IX were seen by Kamio et al. (2005), using SOHO

CDS to observe the gradual rise of the GOES light curve for the flare of 2002 July 29. The time behaviour of these intensities correlated well with the derivative of the GOES light curve during its rise to maximum. In addition there was evidence of down flow in the two transition region lines. All three lines are presumably responding to additional transient non-thermal energy releases during the gradual rise of the main flare plasma signal with enhancement in Mg IX ($T \approx 1$ MK) due to transient heating of the flare plasma. The behaviour we see following the jet is that of gradual non-impulsive selective enhancement in the cooler coronal lines which fits our suggestion of sub-escape velocity jet plasma falling back along open magnetic field lines. The heating due to a shock (if any) produced by falling plasma may be excluded because the field of view of the jet figure does

not include the footpoint of the jet.

The trajectory of the jets will effect the path of the falling-back jet plasma (Wood et al. 1999) which, being in the low plasma-beta regime, must follow magnetic field lines. If the jet is significantly inclined to the vertical, the jet plasma may simply follow a ballistic-like path, or be injected into a loop, with most of the plasma never returning to the point of origin. However, in a coronal hole environment with open magnetic field lines, jets have a high probability of being produced by reconnection between emerging (closed) loops and open field lines. In such cases the resulting jets are likely to be close to the vertical direction. Hence we would expect to find that post jet cool emission line enhancements occur preferentially in coronal hole jets.

Assuming thermal conduction along the jet magnetic axis, the material that fails to escape the Sun, is significantly cooler by the time it returns to the site of the original jet measurement and therefore no longer emits so strongly in the X-ray range. This situation would have arisen for the original Yohkoh SXT jet observations where the telescope response began to fall sharply for temperatures below 2 MK. However the wide temperature coverage of EIS has allowed us to discover this phenomenon. This conclusion is supported by the ability of XRT to detect emission from this lower temperature plasma

due to its greater sensitivity and significantly lower temperature response (down to 1 MK) than that of Yohkoh SXT. In future work we will extend the use of this technique to more detailed studies of the heating and cooling of jet plasma and to the determination of its origins.

Hinode is a Japanese mission developed and launched by ISAS/JAXA, collaborating with NAOJ as domestic partner, NASA and STFC (UK) as international partners. Scientific operation of the Hinode mission is conducted by the Hinode science team organized at ISAS/JAXA. This team mainly consists of scientists from institutes in the partner countries. Support for the post-launch operation is provided by JAXA and NAOJ (Japan), STFC (U.K.), NASA (U.S.A.), ESA, and NSC (Norway). We would like to thank Giulio del Zanna for assistance in calculating the jet electron density estimate. LC thanks the Leverhulme Foundation for an Emeritus Fellowship. DB thanks PPARC for support via PhD studentship. LvDG acknowledges Hungarian government grant OTKA T048961. We acknowledge the substantial effort by the teams at MSSL, NRL, RAL, Birmingham, NAOJ, ISAS/JAXA, and the University of Oslo who made the EIS instrument a reality. Finally we thank the anonymous referee for helpful and insightful comments.

References

- Brooks, D. H., Kurokawa, H., & Berger, T. E. 2007, *ApJ*, 656, 1197
 Culhane, J. L., et al. 2007, *Sol. Phys.*, 243, 19
 Dere, K. P., Landi, E., Mason, H. E., Monsignori Fossi, B. C., & Young, P. R. 1997, *A&AS*, 125, 149
 Golub, L., et al. 2007, *Sol. Phys.*, 243, 63
 Kamio, S., Hara, H., Watanabe, T., Matsuzaki, K., Shibata, K., Culhane, L., & Warren, H. 2007, *PASJ*, 59, S757
 Kamio, S., Kurokawa, H., Brooks, D. H., Kitai, R., & Ueno, S. 2005, *ApJ*, 625, 1027
 Ko, Y.-K., et al. 2005, *ApJ*, 623, 519
 Kosugi, T., et al. 2007, *Sol. Phys.*, 243, 3
 Shibata, K., et al. 1992, *PASJ*, 44, L173
 Shimojo, M., Hashimoto, S., Shibata, K., Hirayama, T., Hudson, H. S., & Acton, L.W. 1996, *PASJ*, 48, 123
 Shimojo, M., & Shibata, K., 2000, *ApJ*, 542, 1100
 Sterling, A. C., Mariska, J. T., Shibata, K., & Suematsu, Y. 1991, *ApJ*, 381, 313
 Sterling, A. C., Shibata, K., & Mariska, J. T. 1993, *ApJ*, 407, 778
 Sterling, A. C., Shibata, K., & Mariska, J. T. 1994, *SSRv*, 70, 77
 Strong, K. T., Harvey, K., Hirayama, T., Nitta, N., Shimizu, T., & Tsuneta, S. 1992, *PASJ*, 44, L161
 Wood, B. E., Karovska, M., Cook, J. W., Howard, R. A., & Brueckner, G. E. 1999, *ApJ*, 523, 444
 Yokoyama, T., & Shibata, K. 1995, *Nature*, 375, 42
 Yokoyama, T., & Shibata, K. 1996, *PASJ*, 48, 353
 Young, P. R., Del Zanna, G., Landi, E., Dere, K. P., Mason, H. E., & Landini, M. 2003, *ApJS*, 144, 135